



Novel nickel(II), palladium(II), and platinum(II) complexes having a pyrrolyl-iminophosphine (PNN) pincer: Synthesis, crystal structures, and cytotoxic activity

Youngwon Kim^a, Jinwook Lee^a, You-Hwa Son^b, Sang-Un Choi^b, Mahboob Alam^c, Soonheum Park^{a,*}

^a Department of Advanced Materials Chemistry, Dongguk University, 123 Dongdae-ro, Gyeongju 780-714, Republic of Korea

^b Center for Drug Discovery Technology, Korea Research Institute of Chemical Technology, 141 Gajeongro, Daejeon 34114, Republic of Korea

^c Division of Chemistry and Biotechnology, Dongguk University, 123 Dongdae-ro, Gyeongju 780-714, Republic of Korea

ARTICLE INFO

Keywords:

PNN-pincer complex
X-ray crystal structure
Cytotoxicity
Apoptosis
DNA cleavage
Molecular docking simulation

ABSTRACT

A pyrrolyl-iminophosphine (PNNH) which would act as a potential terdentate ligand has been prepared by Schiff base reaction. Complexes [M(PNN)X] (M = Ni; X = Cl (1), Pd; X = Cl (2), Br (3), I (4), M = Pt; X = Cl (5)) were prepared. The title complexes were characterized by various spectroscopic (IR, ¹H, ¹³C, and ³¹P NMR) and elemental analyses. The molecular structures of 1, 2, and 5 have been established by single-crystal X-ray crystallography, demonstrating a distorted square planar geometry comprising two 5-membered metallacyclic rings. Complexes 1 and 2 were found to crystallize in the orthorhombic while complex 5 crystallizes in the monoclinic. Cytotoxicities of the complexes along with PNNH were evaluated against A549 (lung), SK-OV-3 (ovarian), SM-MEL-2 (skin), and HCT15 (colon) human cancer cell lines by sulforhodamine B assay. Notably, the palladium(II) complex (2) shows the highest activity. Apoptosis activity along with the caspase inhibitor Z-VAD (Z-Val-Ala-Asp-fluoromethyl ketone) assay of 2 and 5 against A549 and HCT15 cancer cell lines were investigated to learn a mechanistic pathway for the observed cytotoxicity, practically eliminating an apoptotic cell-death route. Complexes 2 and 5 were studied to DNA cleavage assay and molecular docking simulation. The DNA (pcDNA3.0) cleavage experiment evaluates complex 5 interacting with DNA, more effectively, in comparison to complex 2. Molecular docking simulation of 2 and 5 toward DNA and GRP78 (glucose-regulated protein 78) was performed to predict binding sites of ligand-receptors and a plausible mechanistic aspect of metallodrug-action.

1. Introduction

The discovery of cisplatin as a potent antitumor agent initiated the field of pharmaceutical metallodrugs [1]. Despite its high antitumor activity, however, cisplatin has side effects, such as toxicity to normal cells and drug resistance. To solve these problems, cisplatin derivatives have been developed [2–6], and most of the transition metals have been studied in the pharmaceutical field [7]. The development of new anticancer drugs is needed to reduce the side effects and improve efficiency.

The efficacy of metallodrugs is based on the central metal and ligand [8]. Among the transition metals, palladium, which has similar properties to platinum in terms of coordination chemistry, has attracted considerable attention as an alternative to platinum in the development of new anticancer agents. On the other hand, palladium complexes with

monodentate ligands as supporting ligands showed lower anticancer activity than their platinum analogs [9–12]. This suggests that the palladium complexes do not maintain their structure until they reach the pharmacological target in biological fluids because of the rapid ligand-exchange kinetics, which is ~10⁵ times faster than that of the platinum analogs [13,14]. As a way to overcome this high lability, chelate ligands have been used to produce thermodynamically stable and kinetically inert palladium complexes. Palladium complexes with chelate ligands showed high anticancer activity and occasionally higher activity than their platinum analogs [15,16]. The interpretation is that the chelation of metals exhibits high thermodynamic stability, as in the case of palladium and platinum. On the other hand, chelates of platinum are too kinetically inert, whereas the analogs of palladium are kinetically labile. In some cases, these properties of palladium complexes with an appropriate chelating ligand are more suitable for

* Corresponding author.

E-mail address: shpark@dongguk.ac.kr (S. Park).

<https://doi.org/10.1016/j.jinorgbio.2020.111015>

Received 17 December 2019; Received in revised form 23 January 2020; Accepted 27 January 2020

Available online 30 January 2020

0162-0134/ © 2020 Elsevier Inc. All rights reserved.

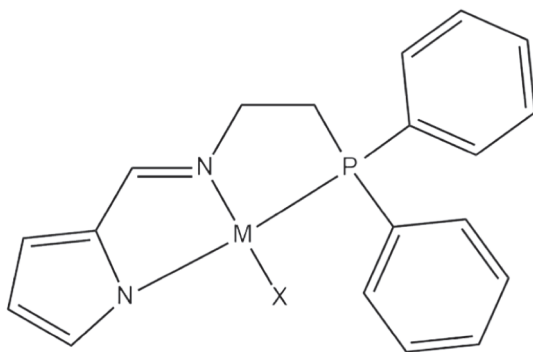
interacting with cancer cells and exhibiting high anticancer activity [17].

Potential terdentate ligands have been developed to prepare pincer-type complexes that have chelating ability to form stable complexes with various transition metal ions [18–24]. Pincer complexes have been studied in many fields [25–27] and demonstrated efficacy in the pharmaceutical field, such as antibacterial [28], antifungal [29], antioxidant [30], and anticancer agents [31–34]. In some cases, although the ligand in itself is active against microorganisms, the incorporation of a transition metal frequently enhances the biological activity, and often decreases the cytotoxicity of both the metal ion and ligand [35–40]. Pincer complexes with various transition metals such as vanadium, iron, nickel, copper, ruthenium, palladium, osmium, platinum, and gold have been studied [41–49]. In particular, pincer complexes of iron, copper, ruthenium, palladium, osmium, platinum and gold showed significantly higher anticancer activity than cisplatin as a positive control. The anticancer activities of the reported pincer complexes against various cancer cell lines, such as AGS (gastric), NCI-H460 (lung), HCT116 (colorectal), HeLa (cervical), Hep G2 (liver), MCF7 (breast), PC3 (prostate), and A172 (glioma), varied according to the central metal ions and ligand frameworks along with structural variations [42,44–49].

The antitumor activity of transition metal complexes can be manifested by various mechanisms. The binding of a metal complex to nucleic acid in DNA is one of the most common causes of its anticancer activity, a typical example of cisplatin. Intracellular aquation of the chloride ligand can generate the active species of cisplatin, forming adducts to the DNA. This binding of cisplatin causes DNA cleavage, damage, and torsion that trigger a cell death mechanism [50,51]. Transition metal complexes can also act as pro-oxidants to produce reactive oxygen species (ROS), such as hydroxyl free radicals, which cause DNA damage (both mitochondria and nuclear) [52–54]. Damage to the mitochondria by ROS discharges mitochondrial cytochrome-C, encouraging the intrinsic death pathway [55].

A recent study showed that a palladium(II) complex with O-donor chelate ligands exhibited anticancer activity in another pathway from the DNA interactions of platinum complexes [56]. This phenomenon induced by the palladium complex is referred to as endoplasmic reticulum (ER) stress, which has been demonstrated to be a cytosolic target and a proapoptotic pathway, being described as the overexpression of glucose-regulated protein 78 (GRP78). In addition, overexpression of GRP78 confronts resistance to chemotherapeutic agents in various cancer cell lines [57].

In this study, a series of novel nickel-triad complexes (Fig. 1) containing a pyrrolyl-iminophosphine (PNN = $\text{PPh}_2(\text{CH}_2)_2\text{N}=\text{CHC}_4\text{H}_3\text{N}$)



M = Ni, Pd, Pt; X = halide

Fig. 1. Target complexes of the nickel-triad having a PNN pincer as anticancer agents.

as a terdentate pincer-type ligand were evaluated their cytotoxic activities against A549 (lung), SK-OV-3 (ovarian), SM-MEL-2 (skin), and HCT15 (colon) human cancer cell lines. Among the title complexes, the palladium(II) and platinum(II) derivatives exhibited excellent activity toward all the cancer cell lines tested. Apoptosis assay in the presence of the complexes, along with a caspase inhibitor Z-VAD, was explored to discuss a cell-death route. DNA cleavage assays of the complexes as well as molecular docking simulation with DNA and GRP78 suggested that the observed cytotoxicities are likely involved different cell-death pathways, depending on the nature of the central metal in the complexes.

2. Experimental

2.1. General methods and materials

All preparations of air-sensitive compounds were carried out on a standard Schlenk line under high purity nitrogen atmosphere. Absolute ethanol was supplied from Hayman Chemical Company and used without purification. Dichloromethane and diethyl ether were used after storing over molecular sieves (4 Å) under N_2 . 2-(Diphenylphosphino)ethylamine from Alfa Aesar, pyrrole-2-carbaldehyde from Aldrich, and triethylamine from Junsei Chemical were purchased and used as supplied. Anhydrous NiCl_2 was from Aldrich and dried at 120 °C in a ventilated oven. PdCl_2 and K_2PtCl_4 were supplied by the Pressure Chemical Company and used as received. All other reagents were acquired from various commercial companies. $\text{Pd}(\text{COD})\text{X}_2$ (X = Cl, Br; COD = 1,5-cyclooctadiene) [58] and $\text{Pt}(\text{SET}_2)\text{Cl}_2$ [59] were prepared according to the literature methods.

2.2. Physical measurements

IR spectra were recorded on a Bruker (Tensor 37) FT-IR spectrometer, as pressed KBr pellets. The ^1H , $^{13}\text{C}\{^1\text{H}\}$, and $^{31}\text{P}\{^1\text{H}\}$ NMR spectra were measured on a Varian Gemini 2000 spectrometer (^1H (199.975 MHz), $^{13}\text{C}\{^1\text{H}\}$ (50,288 MHz), $^{31}\text{P}\{^1\text{H}\}$ (80.950 MHz)) in CDCl_3 at ambient temperature. The chemical shifts for ^1H and $^{13}\text{C}\{^1\text{H}\}$ NMR are reported in parts per million (δ) relative to TMS (Me_4Si) and natural contents of ^{13}C in CDCl_3 , respectively. For $^{31}\text{P}\{^1\text{H}\}$ NMR spectroscopy, the chemical shifts were measured in parts per million relative to external 85% H_3PO_4 in a sealed capillary. Elemental analyses were performed at Korea Basic Science Institute in Seoul, Korea. Biological study of the title compounds on antitumor activity, apoptosis activity, and DNA cleavage were carried out at Korea Research Institute of Chemical Technology in Daejeon, Korea.

2.3. Synthesis

2.3.1. $\text{PPh}_2(\text{CH}_2)_2\text{N}=\text{CHC}_4\text{H}_3\text{NH}$ (PNNH)

Absolute ethanol (30 mL) was bubbled with nitrogen gas for 15 min to eliminate dissolved oxygen. Under nitrogen atmosphere, pyrrole-2-carbaldehyde (0.415 g, 4.36 mmol) was dissolved in bubbled absolute ethanol. To this solution, 2-(diphenylphosphino)ethylamine (1.00 g, 4.36 mmol) was added. The mixture was stirred for 3 h at ambient temperature. White powders of compound $\text{PPh}_2(\text{CH}_2)_2\text{N}=\text{CHC}_4\text{H}_3\text{NH}$ (PNNH) were precipitated during the course of the reaction. The precipitates were filtered under vacuum, washed with cold ethanol, and dried *in vacuo*. Yield 1.22 g (91%). IR: $\nu(\text{NH}) = 3153 \text{ cm}^{-1}$, $\nu(\text{N}=\text{C}) = 1639 \text{ cm}^{-1}$. ^1H NMR (CDCl_3): δ 2.41 t (2H, NCH_2 ; $^3\text{J}(\text{HH}) = 7.7 \text{ Hz}$), δ 3.65 dt (2H, PCH_2 ; $^3\text{J}(\text{HH}) = 8.3 \text{ Hz}$, $^2\text{J}(\text{PH}) = 7.6 \text{ Hz}$), δ 6.21 t (1H, pyrrole), δ 6.43 (1H, pyrrole), δ 6.83 (1H, pyrrole), δ 7.3–7.5 m (10H, phenyl). $^{31}\text{P}\{^1\text{H}\}$ NMR (CDCl_3): δ -19.1 s. $^{13}\text{C}\{^1\text{H}\}$ NMR (CDCl_3): δ 151.74 s (imine, $\text{C}=\text{N}$). Anal. Calcd for $\text{C}_{19}\text{H}_{19}\text{N}_2\text{P}$: C, 74.49; H, 6.25; N, 9.14. Found: C, 74.15; H, 5.98; N, 8.84.

2.3.2. $Ni(PPh_2(CH_2)_2N=CHC_4H_3N)Cl$, $Ni(PNN)Cl$ (**1**)

Absolute ethanol (30 mL) was bubbled with nitrogen gas for 15 min. Under nitrogen atmosphere, $NiCl_2$ (21 mg, 0.163 mmol), $PPh_2(CH_2)_2N=CHC_4H_3NH$ (PNNH) (50 mg, 0.163 mmol), and triethylamine (25 mg, 0.247 mmol) were added into the bubbled absolute ethanol. The reaction mixture was stirred for 3 h at 80 °C, resulting in a reddish solution. The volume of solution was reduced to ca. 5 mL under high vacuum. Diethyl ether (30 mL) was added to the concentrated solution, resulting in red precipitates. The precipitates were filtered under vacuum, washed with distilled water, cold ethanol and diethyl ether, and then dried *in vacuo*. An analytically pure compound of **1** can be obtained by column chromatography (a short glass-column, 0.7 × 15 cm) on silica gel (ca. 2 cm) with CH_2Cl_2 eluent to give red solids from *n*-hexane. Yield 51.4 mg (79%). IR: $\nu(N=C) = 1574\text{ cm}^{-1}$. 1H NMR ($CDCl_3$): δ 2.28 dt (2H, NCH_2 ; $^3J(HH) = 7\text{ Hz}$, $^3J(PH) = 9.8\text{ Hz}$), δ 3.30 dt (2H, PCH_2 ; $^3J(HH) = 6.8\text{ Hz}$, $^2J(PH) = 22.6\text{ Hz}$), δ 6.17 s (1H, pyrrole), δ 6.66 d (1H, pyrrole), δ 7.02 s (1H, pyrrole), δ 7.4–8.1 m (10H, phenyl). $^{31}P\{^1H\}$ NMR ($CDCl_3$): δ 34.3 s. Anal. Calcd for $C_{19}H_{18}N_2ClPNI$: C, 57.13; H, 4.54; N, 7.01. Found: C, 57.05; H, 4.62; N, 6.87.

2.3.3. $Pd(PPh_2(CH_2)_2N=CHC_4H_3N)Cl$, $Pd(PNN)Cl$ (**2**)

A similar procedure as for complex **1**, using $Pd(COD)Cl_2$ (50 mg, 0.175 mmol), PNNH (53.6 mg, 0.175 mmol), and NEt_3 (27.3 mg, 0.269 mmol) gave complex **2** (yellow solids). Yield 63 mg (80%). IR: $\nu(N=C) = 1574\text{ cm}^{-1}$. 1H NMR ($CDCl_3$): δ 2.66 dt (2H, NCH_2 ; $^3J(HH) = 6.7\text{ Hz}$, $^3J(PH) = 10.6\text{ Hz}$), δ 3.64 dt (2H, PCH_2 ; $^3J(HH) = 6.5\text{ Hz}$, $^2J(PH) = 26.8\text{ Hz}$), δ 6.24 s (1H, pyrrole), δ 6.74 s (1H, pyrrole), δ 7.32 s (1H, pyrrole), δ 7.4–8.0 m (10H, phenyl). $^{31}P\{^1H\}$ NMR ($CDCl_3$): δ 46.8 s. $^{13}C\{^1H\}$ NMR ($CDCl_3$): δ 158.71 s (imine, $C=N$). Anal. Calcd for $C_{19}H_{18}N_2ClPPd$: C, 51.02; H, 4.05; N, 6.26. Found: C, 50.50; H, 4.02; N, 6.03.

2.3.4. $Pd(PPh_2(CH_2)_2N=CHC_4H_3N)Br$, $Pd(PNN)Br$ (**3**)

A similar procedure as for complex **1**, using $Pd(COD)Br_2$ (61 mg, 0.163 mmol), PNNH (50 mg, 0.163 mmol), and NEt_3 (27.3 mg, 0.269 mmol) in dichloromethane (10 mL) gave complex **3** (orange solids). Yield 68 mg (85%). IR: $\nu(N=C) = 1575\text{ cm}^{-1}$. 1H NMR ($CDCl_3$): δ 2.67 dt (2H, NCH_2 ; $^3J(HH) = 6.8\text{ Hz}$, $^3J(PH) = 9.8\text{ Hz}$), δ 3.63 dt (2H, PCH_2 ; $^3J(HH) = 6.5\text{ Hz}$, $^2J(PH) = 27\text{ Hz}$), δ 6.22 s (1H, pyrrole), δ 6.76 s (1H, pyrrole), δ 7.42 s (1H, pyrrole), δ 7.5–8.0 m (10H, phenyl). $^{31}P\{^1H\}$ NMR ($CDCl_3$): δ 49.2 s. $^{13}C\{^1H\}$ NMR ($CDCl_3$): δ 158.58 s (imine, $C=N$). Anal. Calcd for $C_{19}H_{18}N_2BrPPd$: C, 46.42; H, 3.69; N, 5.70. Found: C, 46.72; H, 3.75; N, 5.55.

2.3.5. $Pd(PPh_2(CH_2)_2N=CHC_4H_3N)I$, $Pd(PNN)I$ (**4**)

Under nitrogen atmosphere, a mixture of complex **3** (10 mg, 0.02 mmol) and sodium iodide (60.85 mg, 0.4 mmol) was dissolved in acetone (10 mL) and stirred for 3 h at ambient temperature. Removal of all volatiles from the solution under high vacuum gave red-yellow residues, which were washed with distilled water and cold ethanol. The resulting residues were extracted with dichloromethane (10 mL) to give a reddish brown solution. The volume of solution was reduced to ca. 5 mL and poured diethyl ether (30 mL) to give reddish brown powders. The resulting precipitate was filtered under vacuum, washed with distilled water, cold ethanol and diethyl ether, and then dried *in vacuo*. Yield 8 mg (73%). IR: $\nu(N=C) = 1576\text{ cm}^{-1}$. 1H NMR ($CDCl_3$): δ 2.72 dt (2H, NCH_2 ; $^3J(HH) = 6.6\text{ Hz}$, $^3J(PH) = 10.2\text{ Hz}$), δ 3.61 dt (2H, PCH_2 ; $^3J(HH) = 6.4\text{ Hz}$, $^2J(PH) = 26.4\text{ Hz}$), δ 6.18 s (1H, pyrrole), δ 6.76 s (1H, pyrrole), δ 7.5–8.0 m (10H, phenyl). $^{31}P\{^1H\}$ NMR ($CDCl_3$): δ 51.9 s. $^{13}C\{^1H\}$ NMR ($CDCl_3$): δ 158.42 s (imine, $C=N$). Anal. Calcd for $C_{19}H_{18}N_2I PPPd$: C, 42.37; H, 3.37; N, 5.20. Found: C, 42.02; H, 3.43; N, 4.88.

2.3.6. $Pt(PPh_2(CH_2)_2N=CHC_4H_3N)Cl$, $Pt(PNN)Cl$ (**5**)

A similar procedure as for complex **1**, using $Pt(SET_2)Cl_2$ (50 mg,

0.112 mmol), PNNH (34.3 mg, 0.112 mmol), and triethylamine (750 mg, 7.46 mmol) in dichloromethane (15 mL) gave complex **5** as yellow solids. Yield 44.4 mg (74%). IR: $\nu(N=C) = 1570\text{ cm}^{-1}$. 1H NMR ($CDCl_3$): δ 2.61 dt (2H, NCH_2 ; $^3J(HH) = 6.8\text{ Hz}$, $^3J(PH) = 10\text{ Hz}$), δ 3.68 dt (2H, PCH_2 ; $^3J(HH) = 6.4\text{ Hz}$, $^2J(PH) = 23\text{ Hz}$), δ 6.37 s (1H, pyrrole), δ 6.81 s (1H, pyrrole), δ 7.34 s (1H, pyrrole), δ 7.5–8.0 m (10H, phenyl). $^{31}P\{^1H\}$ NMR ($CDCl_3$): δ 23.3 t ($^1J(PtP) = 3584\text{ Hz}$). Anal. Calcd for $C_{19}H_{18}N_2ClPtP$: C, 42.59; H, 3.39; N, 5.23. Found: C, 42.23; H, 3.41; N, 4.98.

2.4. Biological studies

2.4.1. Cytotoxic activity

All the cell line using in this study, that is the human non-small cell lung cancer cell lines A549, ovarian cancer cell line SK-OV-3, skin cancer cell line SK-MEL-2 and colorectal cancer cell line HCT15 were maintained using RPMI1640 (RPMI = Roswell Park Memorial Institute) cell growth medium (Gibco, Carlsbad, CA), supplemented with 5% fetal bovine serum (FBS) (Gibco), and grown at 37 °C in a humidified atmosphere containing 5% CO_2 . The cytotoxicity of the compounds against cultured human tumor cell lines was evaluated by the sulforhodamine B (SRB) method [60]. Each tumor cell line was inoculated over standard 96-well flat-bottom microplates and then incubated for 24 h at 37 °C in a humidified atmosphere of 5% CO_2 . The attached cells were then incubated with the serially diluted each samples. After continuous exposure to the compounds for 72 h, the culture medium was removed from each well and the cells were fixed with 10% cold trichloroacetic acid at 4 °C for 1 h. After washing with tap water, the cells were stained with 0.4% SRB dye and incubated for 30 min at room temperature. The cells were washed again and then solubilized with 10 mM unbuffered Tris base solution (pH 10.5). The absorbance was measured spectrophotometrically at 520 nm with a microtiter plate reader. Each experiment was conducted in triplicate. The IC_{50} values of compounds were calculated by the nonlinear regression analysis.

2.4.2. Apoptosis activity

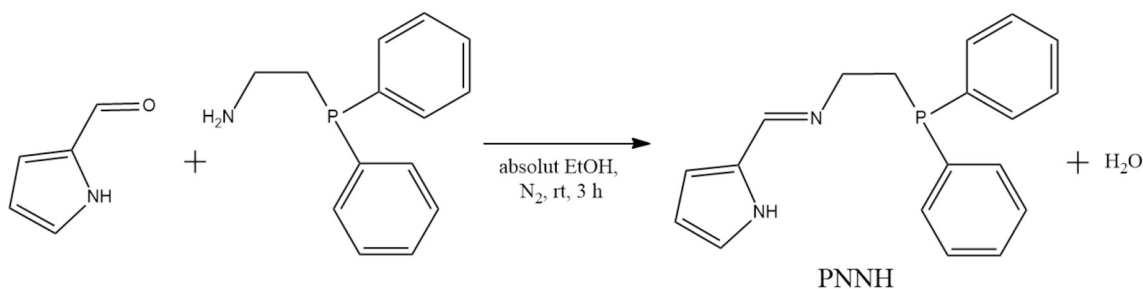
The induced apoptosis ability of complexes **2** and **5** was evaluated in A549 (lung) cancer cells by flow cytometry with annexin V-FITC/PI (fluorescein isothiocyanate/propidium iodide) staining. The A549 cells were seeded in a 6-well plate 1×10^6 per well. After 24 h, various concentrations (0, 0.1, 0.3, and 1 μM) of complexes **2** and **5** were added. After 48 h, cells were washed with cold phosphate-buffered saline (PBS), mixed in $1 \times$ binding buffer at a concentration of 1×10^6 cell/mL. 100 μL of the solution (1×10^5 cells) was transferred to a 5 mL culture tube. The cells were incubated with 5 μL of Annexin V-FITC and 5 μL of PI at room temperature for 15 min in the dark. 400 μL of $1 \times$ binding buffer was added to each tube. The samples were analyzed by flow cytometer within 1 h.

2.4.3. Caspase inhibitor Z-VAD experiment

HCT15 (colon) cancer cells were inoculated over 96-well cell culture plates, and then incubated for 24 h at 37 °C in a humidified atmosphere of 5% CO_2 . Various concentrations (0.3, 1, 3, and 10 μM) of complexes **2** and **5** were added. After 4 h, the culture solution was removed from each well and the cells were washed 3 times with phosphate-buffered saline (PBS). The culture solution containing Z-VAD (30 μM) was added and incubated for 48 h. The cells were photographed.

2.4.4. DNA cleavage experiment

DNA cleavage assays of complexes **2** and **5** with plasmid DNA (pcDNA3.0) were performed by agarose gel electrophoresis. Plasmid DNA aliquots (50 $\mu g/mL$) were incubated in TE buffer (Tris-EDTA; 10 mM Tris-HCl, 1.0 mM EDTA) with 10 μM of complexes **2** and **5** at 25 °C for 24 h. After incubation, the aliquots were subjected to electrophoresis on 1.5% agarose gel in a TAE buffer (Tris Acetate-EDTA;



Scheme 1. Synthesis of pyrrole-iminophosphine $\text{PPh}_2(\text{CH}_2)_2\text{N}=\text{CHC}_4\text{H}_3\text{NH}$ (PNNH).

40 mM Trisacetate, 2.0 mM EDTA). The gel was stained with ethidium bromide before migration. The bands were imaged using a Gel Doc EZ system (Bio-Rad, USA).

2.5. X-ray crystallographic analyses

The X-ray diffraction data for complexes (1, 2, 5) were collected with a Bruker SMART CCD diffractometer equipped with a graphite-monochromated $\text{Mo K}\alpha$ ($\lambda = 0.71073 \text{ \AA}$) radiation source and a nitrogen cold stream ($-100 \text{ }^\circ\text{C}$), at the Western Seoul Center of Korea Basic Science Institute in Seoul, Korea. Data collection and integration were performed with SMART (Bruker, 2000) and SAINT-Plus (Bruker, 2001) [61]. Absorption correction was performed by multi-scan method implemented in SADABS [62]. The structure was solved using direct methods and refined using full-matrix least-squares on F^2 using SHELXTL [63]. All the non-hydrogen atoms were refined anisotropically, and hydrogen atoms were added to their geometrically ideal positions. Crystallographic data for complexes 1 (Ni), 2 (Pd), and 5 (Pt) have been deposited with the Cambridge Crystallographic Data Centre as CCDC 1970178, 1970184, and 1970185, respectively.

2.6. Molecular docking simulation

Molecular docking simulation was performed using a series of software packages such as Mercury, MGLtools (ADT) and Discovery Studio. The crystal data of DNA and protein were retrieved from the Protein Data Bank. The water and associated heteromolecules to the retrieved DNA named 12-mer DNA (PDB code = 1aio) [64] and protein named GRP78 (glucose-regulated protein 78, PDB code = 3ldl) [57] were removed and Gasteiger charges were applied by Autodock Tools (ADT) [65] before performing docking simulation. The PDB format of complexes 2 and 5 were generated by converting CIF files of complexes using Mercury software. The docking site for DNA and protein acting as a receptor was defined by the size of the grid box set at $60 \times 60 \times 60$ in the x, y, and z directions with a grid spacing, 0.375 \AA . Docking was executed employing the Lamarckian genetic algorithm with default parameters and the best pose was chosen on the basis of the binding energy (Kcal/mol). Visualization of the best pose and its interactions was displayed using Discovery Studio.

3. Results and discussion

3.1. Synthesis and characterization

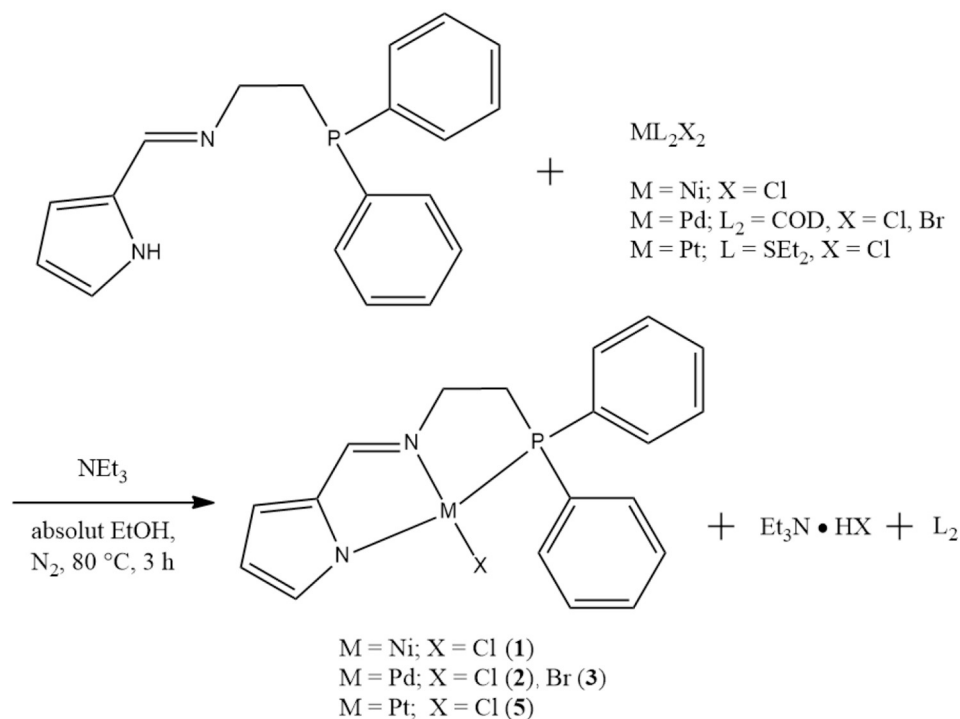
Complexes with labile ligands lead to dissociation of complexes by hydrolysis and/or reaction with a nucleophile in the body. These complications can be overcome using a chelate ligand [14,66,67]. A PNN pincer-type ligand is able to form stable complexes via chelation of P,N,N donors with metal ion. Metal complexes with phosphine ligands exhibit high stability even *in vivo* conditions [68]. In addition, a number of antitumor activities of metal complexes with phosphine ligands have been reported [69–74].

A pyrrole-iminophosphine $\text{PPh}_2(\text{CH}_2)_2\text{N}=\text{CHC}_4\text{H}_3\text{NH}$ (PNNH) has

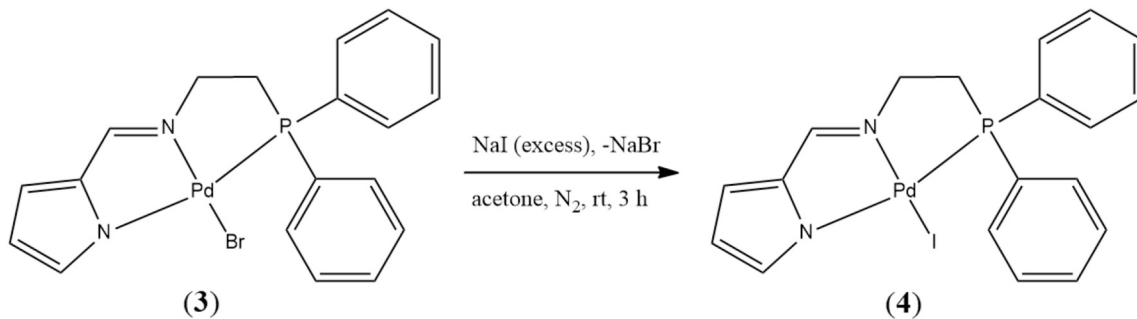
been prepared via Schiff base reaction from pyrrole-2-carbaldehyde and 2-(diphenylphosphino)ethylamine (Scheme 1). PNNH was isolated as white powders in good yields up to 91%. A single resonance at $\delta -19.1$ in the $^{31}\text{P}\{^1\text{H}\}$ NMR spectrum of PNNH ruled out any contamination of phosphine oxide from the reaction. The new complexes $\text{M}(\text{PNN})\text{X}$ ($\text{M} = \text{Ni}$; $\text{X} = \text{Cl}$ (1), $\text{M} = \text{Pd}$; $\text{X} = \text{Cl}$ (2), Br (3), I (4), $\text{M} = \text{Pt}$; $\text{X} = \text{Cl}$ (5), $\text{PNN} = \text{PPh}_2(\text{CH}_2)_2\text{N}=\text{CHC}_4\text{H}_3\text{N}$) have been prepared by reacting the ligand with $(\text{COD})\text{PdCl}_2$, $(\text{COD})\text{PdBr}_2$, NiCl_2 , and $(\text{Et}_2\text{S})_2\text{PtCl}_2$, respectively (Scheme 2). Palladium(II) complex $\text{Pd}(\text{PNN})\text{I}$ (4) has been metathetically prepared from the reaction of complex 3 and NaI (excess) in acetone (Scheme 3). The title complexes 1–5 were characterized by various spectroscopic methods (IR, ^1H , and ^{31}P NMR) including satisfactory microanalytical data (C, H, N). The molecular structures of complexes 1, 2, and 5 have been determined by single crystal x-ray crystallography (*vide infra*: Section 3.2).

In the IR spectrum of the ligand PNNH, the stretching frequency of the $\nu(\text{N}-\text{H})$ and the $\nu(\text{C}=\text{N})$ shows at 3153 cm^{-1} and 1639 cm^{-1} , respectively. These two absorption peaks in the ligand are anticipated to be removed (the $\nu(\text{N}-\text{H})$) and shifted (the $\nu(\text{C}=\text{N})$) upon coordination to metal ion. Complexation of PNNH with the metal ions affords $\eta^3\text{-P,N,N}$ pincer-type complexes consisting of two 5-membered metallacyclic rings ($P\text{-N}(\text{imino})\text{-N}(\text{pyrrolyl})$ pincer, see Fig. 1 and Scheme 2). In the IR spectra of all the title complexes, the absence of $\text{N}-\text{H}$ absorption band clearly indicates that the $\text{N}-\text{H}$ proton in the pyrrole moiety has been removed to be a terdentate ligand, pyrrolylimino phosphine. The characteristic $\nu(\text{C}=\text{N})$ band in the complexes is also shifted to a lower wave number (red shift), compared to that of the free ligand, due to π -back donation of electron density from metal ion to the π^* orbital of imine group. The $\nu(\text{C}=\text{N})$ bands in all complexes were observed at nearby 1570 cm^{-1} (Table S1), indicative of N -coordination of the imine group to the metal ions.

In the ^1H NMR spectrum of PNNH, the resonances of ethylene protons ($\text{CH}_2\text{-CH}_2$) displayed at 3.65 ppm and 2.41 ppm with a quartet and a triplet split-pattern, respectively. Thus the quartet resonance (overlapping with the doublet of the triplet) is due to the one CH_2 protons coupling with phosphorous. In the ^1H NMR spectra of all the metal complexes, the resonance peaks corresponding to the two CH_2 protons in the ethylene group ($\text{NCH}_2\text{-CH}_2\text{P}$) showed their increased coupling constants (δNCH_2 ($^3J(\text{PH})$), δPCH_2 ($^2J(\text{PH})$)) with splitting of double of triplet, respectively (Table S1). In the $^{31}\text{P}\{^1\text{H}\}$ NMR spectrum of PNNH, a single peak resonates at -19.1 ppm. The $^{31}\text{P}\{^1\text{H}\}$ NMR spectra of all the complexes showed their respective single resonance shifted to the downfield, considerably, compared to that of the free ligand. This significant shift to the downfield is partly attributed to the ring formation in the complex, what is called ring shifts [75]. The $^{31}\text{P}\{^1\text{H}\}$ NMR spectrum of the platinum complex (5) shows a single resonance at 23.34 ppm, flanked with platinum satellites ($^1J(\text{PtP}) = 3584 \text{ Hz}$). These phenomena such as the absence of $\text{N}-\text{H}$ absorption peak, the lower shift of the imine absorption peak in the IR spectra, the increased coupling constant values in the ^1H NMR, and downfield shift of phosphorous resonance peak in the $^{31}\text{P}\{^1\text{H}\}$ NMR indicated that the ligand coordinated to the metal ion in a chelate mode. The IR and NMR data are summarized in Table S1.



Scheme 2. Synthesis of $M(PNN)X$ ($M = Ni, Pd, Pt$; $PNN = PPh_2(CH_2)_2N=CHC_4H_3N$).



Scheme 3. Synthesis of $Pd(PNN)I$ (4).

Table 1

Crystal data and structure refinement for 1, 2, and 5.

Compound	Ni(PNN)Cl (1)	Pd(PNN)Cl (2)	Pt(PNN)Cl (5)
Empirical formula	$C_{19}H_{18}ClN_2P Ni$	$C_{19}H_{18}ClN_2P Pd$	$C_{19}H_{18}ClN_2P Pt$
Formula weight	399.48	447.17	535.86
Temperature	200(2) K	200(2) K	223(2) K
Crystal system	Orthorhombic	Orthorhombic	Monoclinic
Space group	$P2_12_12_1$	$P2_12_12_1$	$P2_1/c$
Unit cell dimensions	$a = 11.3120(7)\text{ \AA}$ $b = 12.1276(7)\text{ \AA}$ $c = 12.9257(8)\text{ \AA}$ $\alpha = \beta = \gamma = 90^\circ$	$a = 11.3150(9)\text{ \AA}$ $b = 12.1391(9)\text{ \AA}$ $c = 13.0906(10)\text{ \AA}$ $\alpha = \beta = \gamma = 90^\circ$	$a = 14.8417(16)\text{ \AA}$ $b = 10.9952(11)\text{ \AA}$ $c = 11.1886(11)\text{ \AA}$ $\alpha = \gamma = 90^\circ, \beta = 99.921(4)^\circ$
Volume	$1773.24(19)\text{ \AA}^3$	$1798.0(2)\text{ \AA}^3$	$1798.5(3)\text{ \AA}^3$
Z	4	4	4
Density (calculated)	1.496 Mg/m^3	1.652 Mg/m^3	1.979 Mg/m^3
Absorption coefficient	1.337 mm^{-1}	1.272 mm^{-1}	8.041 mm^{-1}
F(000)	824	896	1024
Crystal size	$0.18 \times 0.10 \times 0.04\text{ mm}^3$	$0.12 \times 0.08 \times 0.03\text{ mm}^3$	$0.190 \times 0.160 \times 0.060\text{ mm}^3$
Theta range for data collection	2.30 to 28.29° .	2.29 to 28.29° .	2.617 to 28.321° .
Reflections collected	12,586	13,011	52,371
Independent reflections	4334 [R(int) = 0.0293]	4431 [R(int) = 0.0387]	4469 [R(int) = 0.0496]
Completeness to theta = 28.29°	99.5%	99.7%	99.9%
Data/restraints/parameters	4334/0/217	4431/0/217	4469/0/217
Goodness-of-fit on F^2	1.143	1.143	1.070
Final R indices [$I > 2\sigma(I)$]	$R1 = 0.0322, wR2 = 0.0640$	$R1 = 0.0354, wR2 = 0.0631$	$R1 = 0.0181, wR2 = 0.0395$
R indices (all data)	$R1 = 0.0486, wR2 = 0.0839$	$R1 = 0.0593, wR2 = 0.0931$	$R1 = 0.0240, wR2 = 0.0429$
Absolute structure parameter	$-0.007(15)$	$-0.02(5)$	
Largest diff. peak and hole	0.460 and $-0.530\text{ e}\text{-}\text{\AA}^{-3}$	1.050 and $-0.814\text{ e}\text{-}\text{\AA}^{-3}$	0.895 and $-0.613\text{ e}\text{-}\text{\AA}^{-3}$

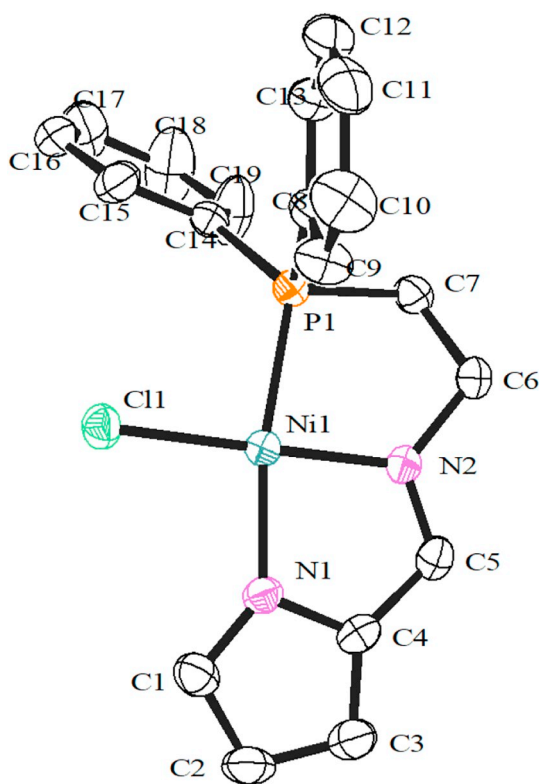


Fig. 2. ORTEP representation of Ni(PNN)Cl (1) with 50% probability ellipsoids. All hydrogens were omitted for clarity.

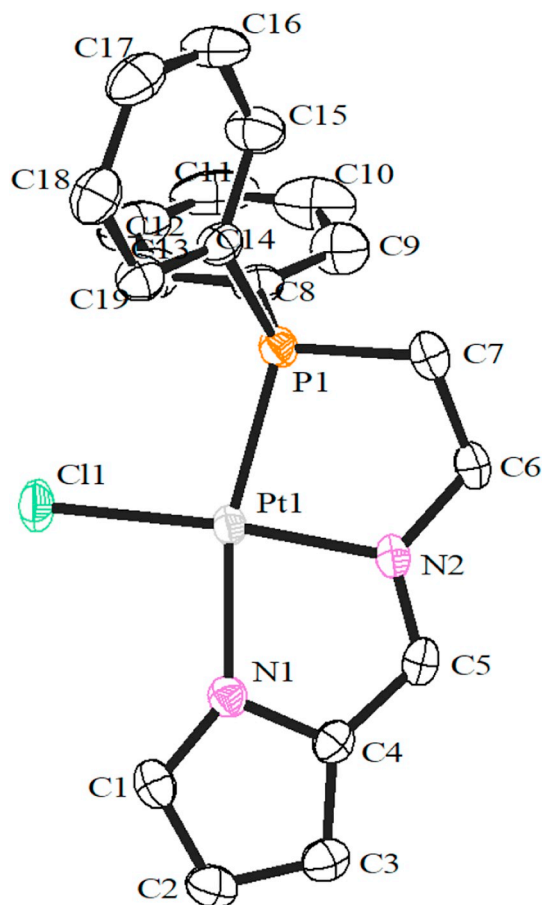


Fig. 4. ORTEP representation of Pt(PNN)Cl (5) with 50% probability ellipsoids. All hydrogens were omitted for clarity.

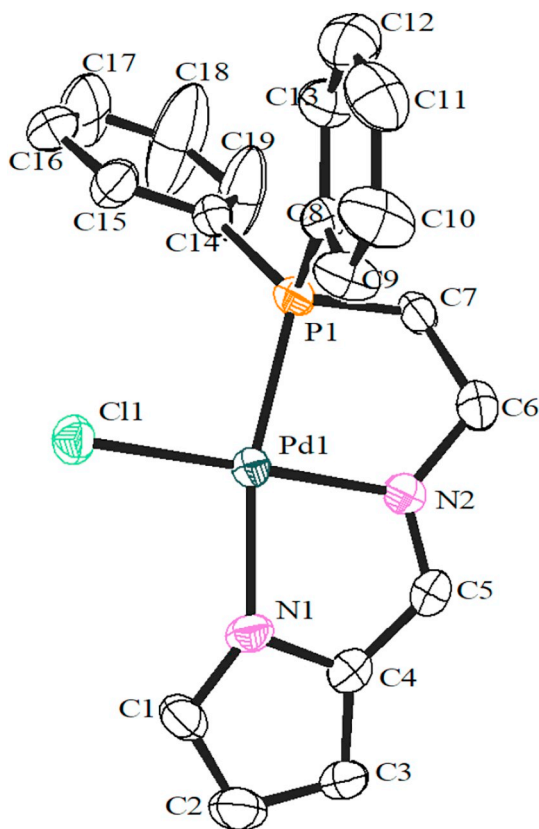


Fig. 3. ORTEP representation of Pd(PNN)Cl (2) with 50% probability ellipsoids. All hydrogens were omitted for clarity.

Microanalytical data for PNNH and complexes (1–5) are all in good agreement with calculated values (Table S2).

3.2. Single crystals X-ray diffraction studies

The molecular structures of complexes 1, 2, and 5 have been established by single crystal x-ray diffraction. Single crystals suitable for an x-ray diffraction study were grown by slow diffusion of *n*-hexane into a dichloromethane solution of the respective complex. Crystal data and structure refinements for 1, 2, and 5 are listed in Table 1. The molecular structures of 1, 2, and 5, shown in Figs. 2, 3, and 4,

Table 2

Selected bond lengths (Å), bond angles (°), and torsion angles (°) for complexes 1, 2, and 5.

	1	2	5
M-N(1)	1.908(2)	2.062(4)	2.044(2)
M-N(2)	1.880(3)	2.006(5)	1.994(2)
M-P(1)	2.1550(9)	2.2280(15)	2.2142(7)
M-Cl(1)	2.1694(8)	2.3080(15)	2.3099(7)
N(2)-C(5)	1.292(4)	1.296(7)	1.299(4)
N(1)-C(1)	1.339(4)	1.331(7)	1.345(4)
N(1)-C(4)	1.383(4)	1.397(7)	1.386(4)
N(2)-M-N(1)	83.50(11)	80.78(19)	79.93(9)
N(2)-M-P(1)	85.48(9)	84.19(14)	85.40(7)
P(1)-M-Cl(1)	94.47(3)	96.94(6)	99.62(3)
N(1)-M-Cl(1)	97.15(8)	98.42(14)	95.22(7)
N(2)-M-Cl(1)	173.74(9)	175.57(15)	173.79(7)
N(1)-M-P(1)	167.41(8)	164.19(14)	165.03(7)
N(2)-C(6)-C(7)-P(1)	43.4(3)	45.4(5)	-40.3(3)

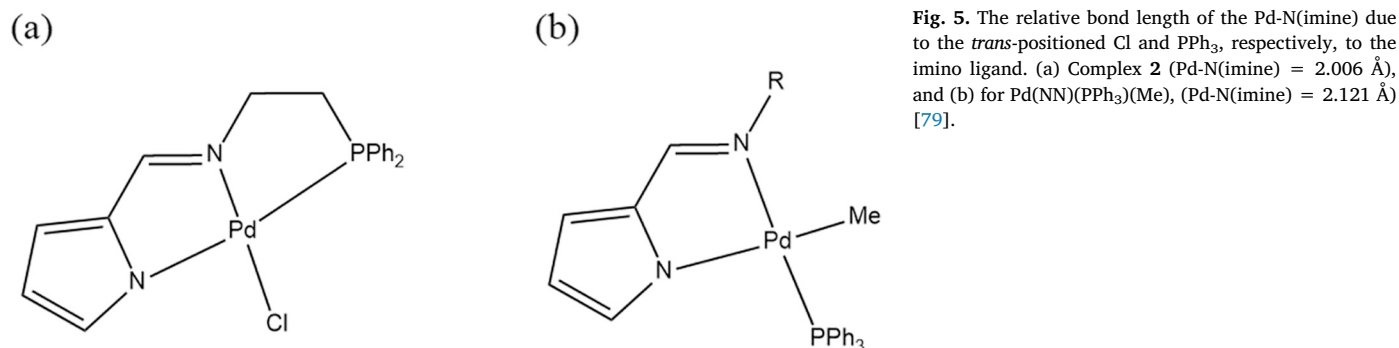


Fig. 5. The relative bond length of the Pd-N(imine) due to the *trans*-positioned Cl and PPh₃, respectively, to the imino ligand. (a) Complex **2** (Pd-N(imine) = 2.006 Å), and (b) for Pd(NN)(PPh₃)(Me), (Pd-N(imine) = 2.121 Å) [79].

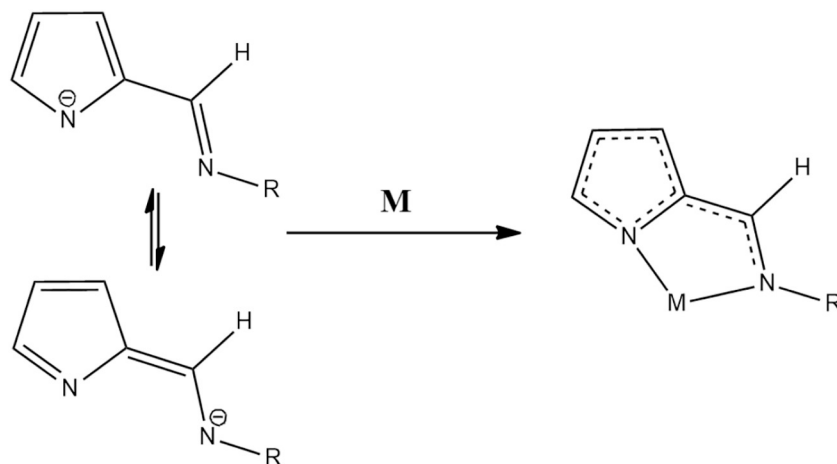


Fig. 6. Resonance forms of pyrrolide-imine ligand and its complex [81].

Table 3

Cytotoxic activity of cisplatin, PNNH, and compound **1–5** against A549 (lung), SK-OV-3 (ovarian), SM-MEL-2 (skin), and HCT15 (colon) human cancer cell lines.

Compound	IC ₅₀ (μM) ± SD ^a			
	A549	SK-OV-3	SM-MEL-2	HCT15
Cisplatin	0.17 ± 0.087	1.55 ± 0.329	0.19 ± 0.14	0.68 ± 0.95
PNNH	> 30	> 30	> 30	> 30
1	> 30	> 30	> 30	> 30
2	0.22 ± 0.21	1.23 ± 0.700	0.53 ± 0.53	0.14 ± 0.088
3	0.36 ± 0.41	1.20 ± 0.618	0.76 ± 0.62	0.18 ± 0.14
4	3.90 ± 3.59	10.02 ± 6.940	10.48 ± 5.065	4.26 ± 3.64
5	2.56 ± 2.13	4.97 ± 2.58	2.52 ± 1.48	2.00 ± 1.66

^a SD is standard deviation of the value.

respectively, illustrate a distorted square planar geometry comprising two 5-membered metallacyclic rings via *P,N,N*-chelation of a pincer-type pyrrolyliminophosphine (*P,N,N* = PPh₂(CH₂)₂N=CHC₄H₃N) ligand. Crystals of complexes **1** and **2** are isomorphous, differing for the ionic radii of Ni²⁺ and Pd²⁺ in the square planar complexes of 63 and 78 pm, respectively, that alter the bond lengths and angles of atoms directly associated with the central metal atoms. The bond lengths and angles for these isomorphous complexes are presented in Table 2 for comparison.

In complex **2**, bond angles along with torsion angles exhibit a slight distorted square-planar geometry mainly arising from the formation of two five-membered palladacyclic rings [76]. The bond length of Pd(1)-N(1) and Pd-N(2) in complex **2** is 2.062(4) and 2.006(5) Å, respectively. The Pd(1)-N(2)(imine) is shorter than the Pd(1)-N(1)(pyrrolyl). This result is consistent with precedents of nickel(II) and palladium complexes bearing an imino-pyrrolyl ligand. The M-N(imine) bond length is shorter than the M-N(pyrrolyl) [77]. However an opposite tendency in those bond lengths in a pyrrolide-imine based titanium complex has

been reported; the Ti-N(pyrrole) is shorter than the Ti-N(imine) [78]. The difference from these two bond lengths observed in pyrrolide-imine based complexes is ascribed mainly to the *trans*-influence. A pyrrolide-imine based palladium(II) complex Pd(NN)(PPh₃)(Me) in which the phosphine and the methyl ligand coordinated to the corresponding *trans*-position of the *N* of the imine and the pyrrole, respectively, has been reported (Fig. 5(b)) [79]. In Pd(NN)(PPh₃)(Me), the bond length of the Pd-N(imine) is 2.121 Å which is longer than that of the Pd-N(imine) (2.006 Å) in complex **2**. In complexes **1** and **5**, nickel(II) and platinum(II) analogs, a similar trend in the relative bond lengths of the M-N(imine) and the M-N(pyrrolyl) have been observed as for those of the palladium complex **2** (see Table 2). The respective bond length of M-N(imine), M-N(pyrrolyl), and M-P in the complexes are in the order of **1** < **5** < **2**. This sequence corresponds to an order of nickel (63 pm), platinum (74 pm), and palladium (78 pm) in the ionic radius of the square planar of metal 2+ oxidation state [80]. On the other hand, the M-Cl bond lengths are in the order of **1** < **2** < **5**. This can be attributed to the elongated N(2)-C(5) (imine) bond length observed in

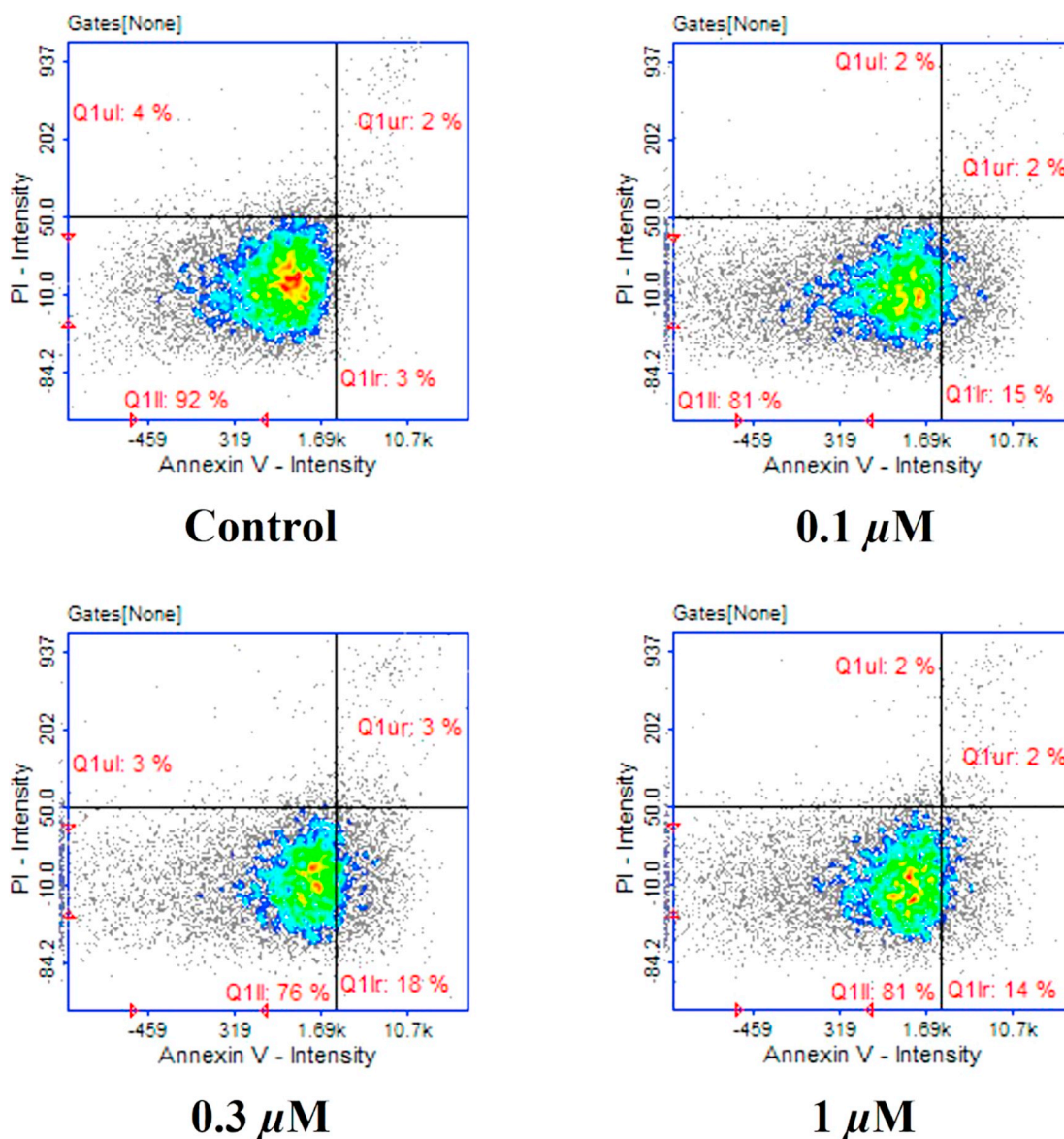


Fig. 7. Apoptosis of A549 (lung) cancer cells with complex 2. Percentage of cells in each quadrant are given as live (lower left), early apoptotic (lower right), late apoptotic (upper right), necrotic cells (upper left).

complex 5. An increasing electron density on the central metal leads to strong π -back donation to the imine group, which may weaken the C=N imine bond followed by the M-N (imine) bond stronger, resulting in elongation of the M-Cl bond length.

In the pyrrolyl ring of complex 2, the C-C bond lengths of C(1)-C(2), C(2)-C(3), and C(3)-C(4) are nearly all the same of 1.39 Å within the standard deviations. But the C-N bond lengths are quite different each other as of the N(1)-C(1) (1.331 Å) and the N(1)-C(4) (1.397 Å). Han et al. suggested that the difference in the bond lengths of the N(1)-C(1) and the N(1)-C(5) in the pyrrole group of a pyrrolide-imine based complex is due to electron delocalization in N(1)-C(4)-C(5)-N(2) [77]. A theoretical study on density functional theory (DFT) for a pyrrole-imine aluminum complex reported by Huang et al. revealed that resonance of the pyrrole-imine ligand in the complex occurs across the entire range from the pyrrole ring to imine group (see Fig. 6) [81]. In this study for complex 2, the structural phenomena for delocalization of the electrons in the pyrrole ring including the imino group, judged from the related bond lengths, is consistent with precedents. Structural similarity of complexes 1 and 5 is analogous to complex 2. The selected

bond lengths (Å), angles (°), and torsion angles (°) for complexes 1, 2, 5 are listed in Table 2.

3.3. Biological studies

3.3.1. Cytotoxic activity

The cytotoxic activities of PNNH and the title complexes were evaluated against A549 (lung), SK-OV-3 (ovarian), SM-MEL-2 (skin), and HCT15 (colon) human cancer cell lines by using SRB (sulforhodamine-B) assay. Cisplatin was used as a positive control. Cytotoxicity data are summarized in Table 3.

As shown in Table 3, PNNH and nickel(II) complex (1) exhibited negligible activity with IC_{50} values of > 30 μ M. However, the palladium complexes (2-4) and the platinum complex (5) were found to be highly active toward all the tested cancer cell lines. Among those, the chloropalladium complex Pd(PNN)Cl (2) showed the highest cytotoxicity against all the cancer cell lines. For HCT15 and SK-OV-3 cell lines, IC_{50} values of the palladium complex (2) are even low in comparison with those of cisplatin. On the other hand, the palladium complex (2) is

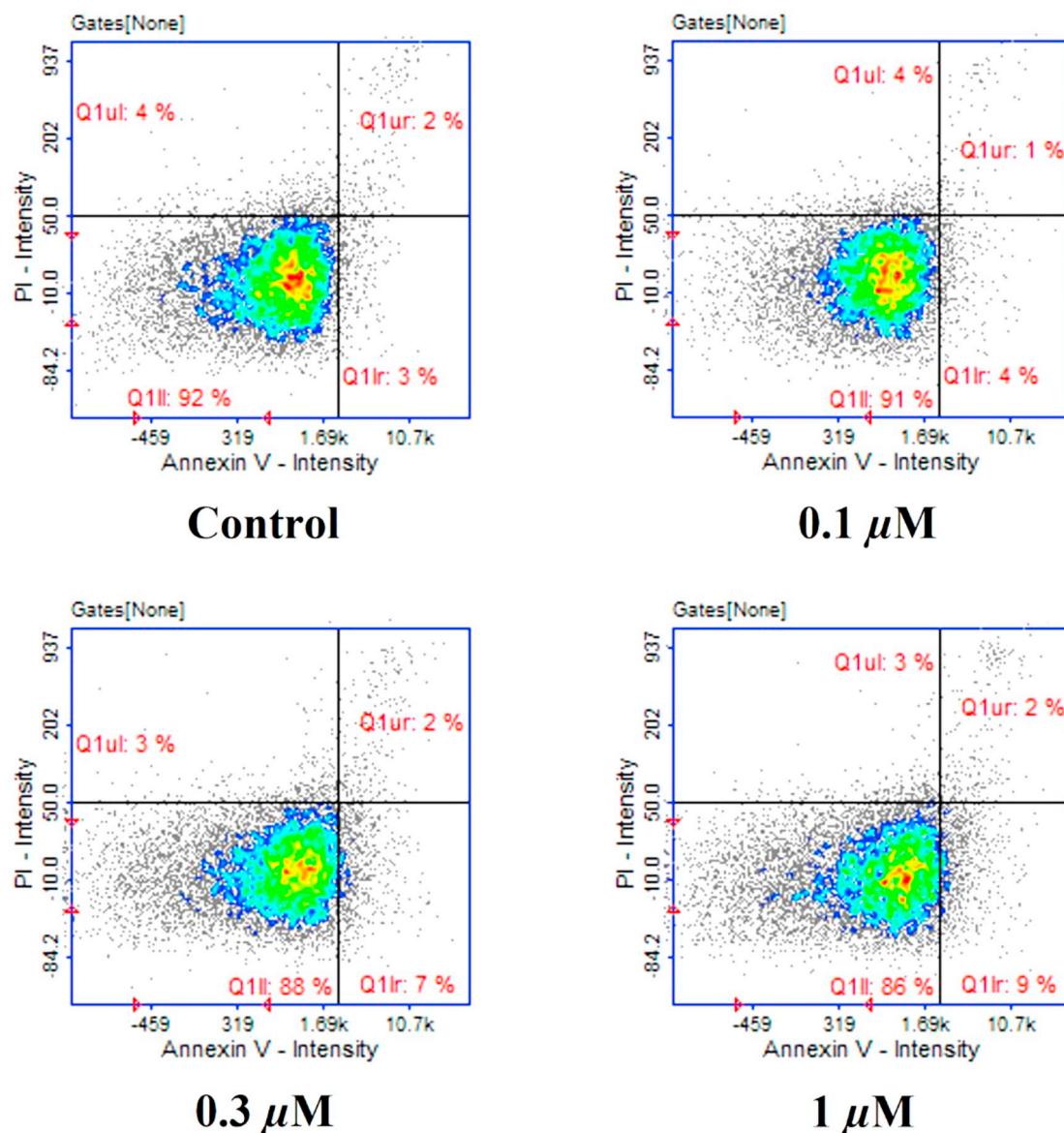


Fig. 8. Apoptosis of A549 (lung) cancer cells with complex 5. Percentage of cells in each quadrant are given as live (lower left), early apoptotic (lower right), late apoptotic (upper right), necrotic cells (upper left).

nearly comparable with cisplatin in IC_{50} values for A549 and SM-MEL-2 cell lines. Comparing cytotoxic activities of the palladium halides (2–4), the chloro and the bromo derivatives (2, 3) showed relatively high activity than the iodo derivative 4. This consequence can be explained by high lability of the iodide ligand than the chloride or the bromide in the complex, likely resulting in a less active palladium species. Furthermore, the palladium chloride 2 shows cytotoxicity of 4 times higher than that of the platinum chloride 5 against all the cancer cell lines tested. Considering significantly different cytotoxic activities resulted from the chloro derivatives of the nickel triad having a PNN pincer (1, 2, 5), the employed central metal is to be critical in efficacy of anticancer metallodrugs [82–84].

3.3.2. Apoptosis assay

Apoptosis, commonly referred to a programmed cell death, contributes to the homeostasis of multicellular organisms by eliminating aged, damaged, and/or abnormal cells. Apoptotic activity has been studied as a factor of anticancer activity of pharmaceuticals [85,86]. Apoptosis begins when phosphatidylserine (PS) inside a plasmic membrane is expressed, externally. Early apoptosis can be confirmed by

detecting the Annexin V binding to PS. The DNA-binding fluorescent dye propidium iodide (PI) cannot penetrate membranes of live cells. However, PI can stain DNA, owing to loss of cell membranes as apoptosis progresses, enabling confirmation of late apoptosis or necrosis [87]. A549 (lung) cancer cells were treated with various concentrations (0, 0.1, 0.3, 1.0 μM) of complexes 2 and 5 for 48 h. Annexin V and PI binding to apoptotic cells were analyzed by flow cytometry to evaluate the apoptotic effects of complexes 2 and 5.

As shown in Fig. 7, treatment with 0.1 μM of complex 2 resulted in 15% of early apoptotic and 2% of late apoptotic cells. However, the observed percentages of early and late apoptotic cells were practically comparable as concentration of complex 2 increases (0.3 and 1.0 μM). The apoptosis results of complex 5 showed 4%, 7%, and 9% in early apoptotic cells at concentration of 0.1, 0.3, and 1.0 μM of the complex, respectively, as shown in Fig. 8. Apoptotic activity was slightly increased in proportion to the concentration of the complex but was less than complex 2. These results demonstrate that an apoptotic cell-death pathway is not considerably responsible for the observed cytotoxic activity of the complexes, likely comprising other cell-death pathways.

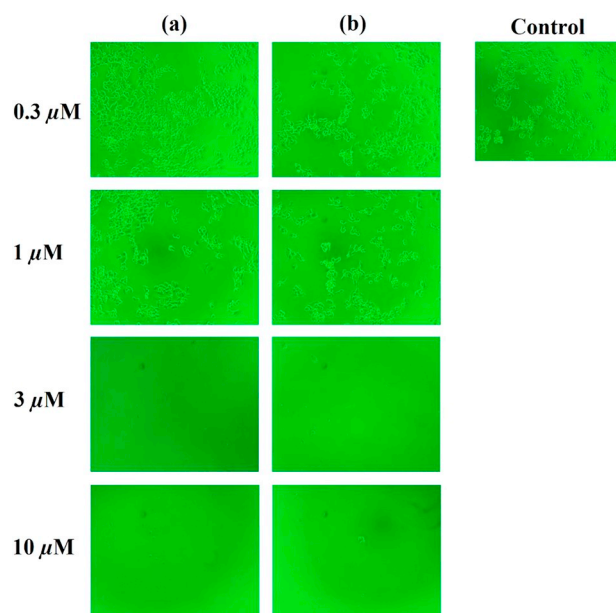


Fig. 9. Image of HCT 15 (colon) cancer cells untreated (a) and treated (b) with 30 μM of Z-VAD after treatment with various concentrations of complex 2.

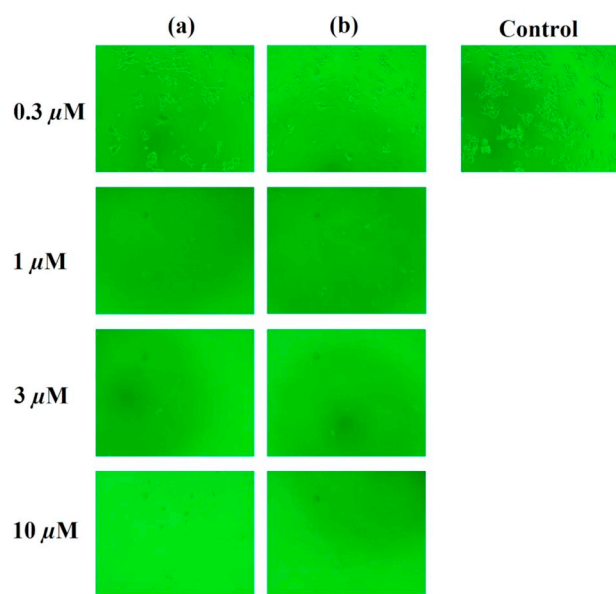


Fig. 10. Image of HCT 15 (colon) cancer cells untreated (a) and treated (b) with 30 μM of Z-VAD after treatment with various concentrations of complex 5.

3.3.3. Z-VAD assay

Apoptosis is mainly expressed by means of activated caspase through intrinsic and extrinsic pathways. An intrinsic pathway is triggered by loss of mitochondrial membranes, releasing cytochrome C from mitochondria, which activates caspase [88]. On the other hand, an extrinsic pathway involves both TRADD (TNF receptor-associated death domain) and FADD (Fas-associated death domain) arising from activation of TNF (tumor necrosis factor) receptor family in membrane. FADD activates caspase, followed by apoptosis [89]. Z-VAD inhibits apoptosis induced by caspase activation, confirming cytotoxicity of the complexes attributable to caspase stimulus [90]. Thus, Z-VAD assay was performed to learn whether the observed cytotoxic activities of complexes 2 and 5 involve an apoptotic pathway induced by caspase activation.

Figs. 9 and 10 are the photographs of colon cancer cells untreated (a) and treated (b) with Z-VAD after treatment with each of various concentrations of complexes 2 and 5. In Fig. 9, the cells treated with 0.3 and 1.0 μM of complex 2 shows a similar amount of living cells, which was treated (a) or untreated (b) with 30 μM of Z-VAD. Moreover, the cells treated with 3.0 and 10 μM of complex 2 displays most of the cancer cells dead whether treated or untreated with Z-VAD. The results with complex 5 also shows that the cytotoxic activity is independent on treatment with caspase-inhibitor Z-VAD as similar to that of complex 2 (Fig. 10).

These results suggest that complexes 2 and 5 exhibit cytotoxic activity through other pathways rather than apoptosis. Apoptosis and necroptosis can be expressed through activation pathways of the TNF receptor family. Activation of TNF receptor by means of TNF α -signals releases TRADD which recruits RIPK1 (receptor-interacting protein kinase 1). In case, caspase is inhibited, RIPK1 associates with RIPK3 to form necrosomes. The necrosome facilitates phosphorylation of MLKL (mixed lineage kinase domain like pseudokinase), which can express necroptosis, as a caspase-independent pathway, leading to cell-death [91]. Consequently, the results of Z-VAD assay may imply that cytotoxicity of complexes 2 and 5 likely involves a pathway of necroptosis, which is another programmed cell-death pathway occurring apoptosis suppressed.

3.3.4. DNA cleavage

Relative interaction of the chloro complexes of palladium(II) (2) and platinum(II) (5) with DNA has been investigated by monitoring the matching bands of a supercoiled DNA (Form I), a nicked DNA (Form II), and a linear DNA (Form III) resulted from a Plasmid DNA (pcDNA 3.0) after treatment with the respective metal complex.

The experimental result from DNA cleavage measured by agarose gel electrophoresis shows detached bands in the order of Form II, Form III, and Form I from top to bottom. DNA cleavage ability of complexes is proportional to an increasing amount of the resulting Form II and Form III. Fig. 11 shows a photograph for the bands from electrophoresis of DNA treated with 10 μM of the respective complex 2 and 5 for 48 h. The

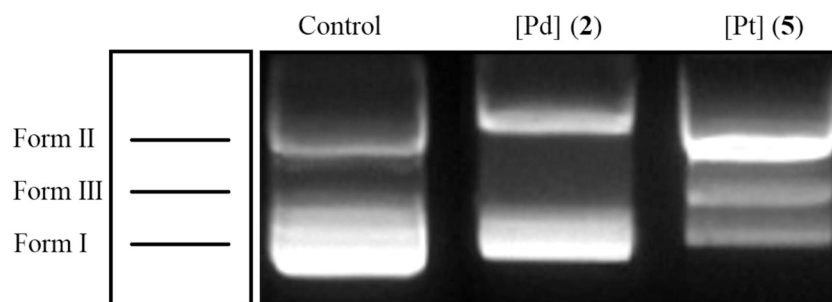


Fig. 11. Cleavage of pcDNA3.0 by complexes 2 and 5 (Control = pcDNA 3.0 (untreated), Form I: supercoiled DNA, Form II: nicked DNA, Form III: linear DNA).

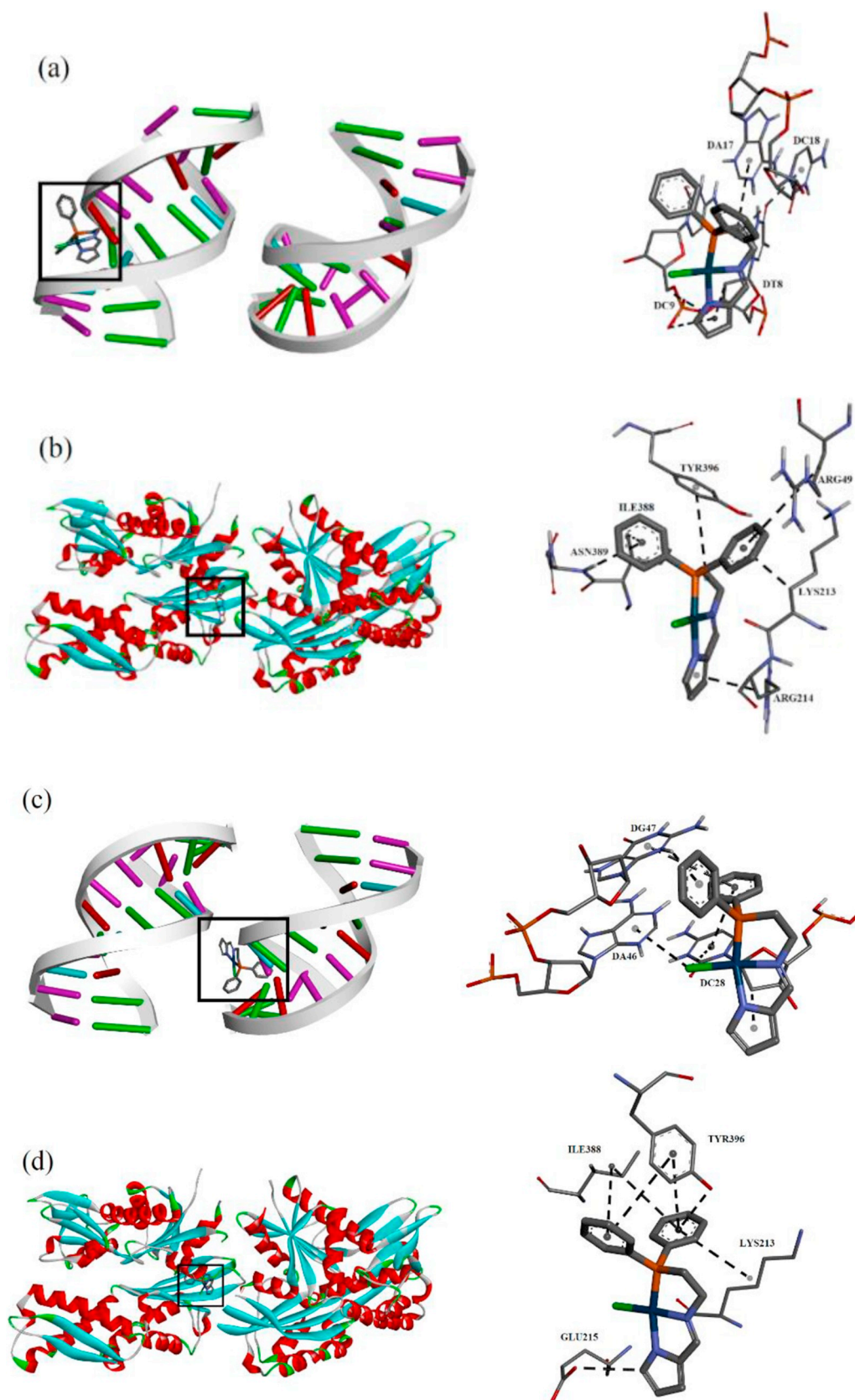


Fig. 12. Interactions of complexes 2 and 5 with receptors: 2 with DNA (a), 2 with GRP78 (b), 5 with DNA (c), and 5 with GRP78 (d).

result shows that the amount of Form I decreased and those of Form II and Form III increased by treatment of the platinum complex (5). On the other hand, the Form II fragments slightly increased by treatment of

the palladium analog (2) compared to the control. This result demonstrates that the platinum complex interacts with plasmid DNA more effectively than the palladium analog does. Consequently, the platinum

Table 4
Thermodynamic data resulted from molecular docking simulation of complexes **2** and **5** toward DNA and GRP78.

	DNA		GRP78	
	ΔG^a	K_i^b	ΔG^a	K_i^b
2	-5.86	50.8	-7.63	2.56
5	-5.94	44.4	-7.44	3.53

ΔG and K_i are the free energy of binding and inhibition constant, respectively.

^a kcal/mol.

^b μ M.

complex likely involves a DNA interaction pathway while the palladium analog does an alternative, considering from the observed cytotoxic activity of the two complexes against the cancer cell lines.

3.4. Molecular docking simulation

The synthesized metal complexes were studied to determine the binding affinity of the crystal structure of human GRP78 (PDB 3LDL) and the crystal structure of double-stranded DNA (PDB 1AIO) in order to discover the interaction between the studied complexes and the receptor, and for lead optimization using molecular docking study. To find out how complexes interact with active sites of receptor and the difference between palladium and platinum complexes with the same ligand, complexes **2** and **5** were simulated with DNA and GRP78.

As shown in Fig. 12(a), there are various types of non-covalent interactions of complex **2** with DNA. The π -electrons of DA17 and DC18 aryl rings in DNA interact with the ethylene protons in the PNN ligand of the complex *via* π -alkyl interaction. The π -electrons of the pyrrolyl moiety in the complex interact with the O-anion and the C5 of DC9, and with the C2 of DT8 in DNA *via* π -anion(O) and π -sigma interaction, respectively. Fig. 12(b) shows interactions of complex **2** with GRP78, revealing that there are similar non-covalent interactions such as the π -alkyl and the π -sigma along with hydrogen bonding of π -HN (ASN389). Detailed interaction types and distances obtained from the molecular docking simulation of complex **2** with DNA and GRP78 are shown in Table S3.

Similarly, Fig. 12 shows molecular interactions resulted from molecular docking simulation of the platinum(II) complex **5** with the same receptors of DNA (c) and GRP78 (d), elucidating that there are comparable covalent interactions such as π -alkyl, π -sigma, and π -hydrogen, as observed from the interactions of the palladium analog **2**. In addition to these types of interactions, intermolecular π - π interactions have been observed from associates of phenyl ring moieties in the complex with DC28 and DG47 in DNA (π - π stacked), and with TYR396 in GRP78 (π - π T-shaped) as well (Table S4).

The thermodynamic values of ΔG (free energy of binding) and K_i (inhibition constant) obtained from molecular docking simulation of complex **2** with DNA and GRP78, respectively, are of -5.86 and -7.63 kcal/mol for ΔG , and are of 50.8 and 2.56 μ M for K_i (Table 4). The respective value of ΔG and K_i for complex **5** with the receptors is of -5.94 kcal/mol along with 44.4 μ M (toward DNA), and is of -7.44 kcal/mol along with 3.53 μ M (toward GRP78). The resulting thermodynamic values reveal that complex **2** is more interactive to GRP78 than DNA as of $\Delta G = -2$ kcal/mol along with 20 times lower inhibition constant. However, the values of ΔG and K_i toward DNA show that the platinum complex **5** has lower binding energy, indicating stronger interaction, than the palladium analog **2**, at different interacting sites in DNA.

Considering from the thermodynamic values for complexes **2** and **5** toward DNA, the platinum complex is more interactive than the palladium complex. However, the two complexes are opposite each other toward GRP78. This result is in agreement with those of the DNA cleavage experiment (*vide supra*, Fig. 11). Thus, the results from MDS

(molecular docking simulation) and DNA cleavage experiment may imply that the palladium species likely proceeds in a different pathway from the platinum in the observed cytotoxicity, *i.e.* the palladium prefers interacting with proteins rather than DNA, while the platinum does the other way. In the observed cytotoxicity, the platinum complex shows less active than the palladium analog against all the cancer cell lines (Table 3). The thermodynamic data resulted from molecular docking simulation of complexes **2** and **5** are summarized in Table 4.

4. Conclusions

In the present study, novel nickel(II), palladium(II), and platinum(II) complexes having a PNN-pincer have been synthesized and characterized by various spectroscopic methods (IR, ^1H and $^{31}\text{P}\{^1\text{H}\}$ NMR) and elemental analysis. The molecular structures of M(PNN)X (M = Ni; X = Cl (**1**), M = Pd; X = Cl (**2**), and M = Pt; X = Cl (**5**), PNN = PPh₂(CH₂)₂N=CHC₄H₃N) were determined by single crystal x-ray crystallography. The cytotoxicity of the synthesized metal complexes against human cancer cell lines (A549, SK-OV-3, SM-MEL-2, and HCT15) was evaluated in a comparative manner. The general trends were found as follows: **2** (Pd-Cl) > **3** (Pd-Br) > **4** (Pd-I) and **2** (Pd-Cl) > **5** (Pt-Cl) \gg **1** (Ni-Cl). In addition, the study of apoptotic activity and caspase inhibitor (Z-VAD) experiments, with complexes **2** and **5** against A549 and HCT15 cancer cells, demonstrates that an apoptosis pathway would not be fully accountable for the observed cytotoxicity, probably involving other pathways. The DNA cleavage experiment demonstrates that the platinum complex (**5**) interacts with a plasmid DNA more effectively than the palladium analog (**2**) does. These results imply that the palladium analog likely involves an alternative pathway in the observed cytotoxicity. In order to investigate the interaction of complexes with proteins and DNA, molecular docking studies were performed, showing that docking energy-based anti-cancer activities of **2** and **5** are consistent with experimental results.

Declaration of competing interest

The authors declare that they have no known competing financial interests or personal relationships that could have appeared to influence the work reported in this paper.

Acknowledgments

This work was supported by the Dongguk University Research Fund of 2019.

Appendix A. Supplementary data

Supplementary data to this article can be found online at <https://doi.org/10.1016/j.jinorgbio.2020.111015>.

References

- [1] B. Rosenberg, L. van Camp, J.E. Trosko, V.H. Mansour, Nature 222 (1969) 385–386.
- [2] A.H. Calvert, S.J. Harland, D.R. Newell, Z.H. Siddik, A.C. Jones, T.J. McElwain, S. Raju, E. Wiltshaw, I.E. Smith, J.M. Baker, M.J. Peckham, K.R. Harrap, Cancer Chemother. Pharmacol. 9 (1982) 140–147.
- [3] C.R. Culy, D. Clemett, L.R. Wiseman, Drugs 60 (2000) 895–924.
- [4] J.R. Eckardt, D.L. Bentsion, O.N. Lipatov, I.S. Polyakov, F.R. MacKintosh, D.A. Karlin, G.S. Baker, H.B. Breitz, J. Clin. Oncol. 27 (2009) 2046–2051.
- [5] R. Duncan, Adv. Drug Deliv. Rev. 61 (2009) 1131–1148.
- [6] J.Q. Zhang, K. Li, K.M. Jiang, Y.W. Cong, S.P. Pu, X.G. Xie, Y. Jin, J. Lin, RSC Adv. 6 (2016) 17074–17082.
- [7] M. Marloye, G. Berger, M. Gelbeke, F. Dufresne, Future Med. Chem. 8 (2016) 2263–2286.
- [8] K.S. Neethu, J. Eswaran, M. Theetharappan, N.S.P. Bhuvanesh, M.A. Neelakantan, K.M. Velusamy, Appl. Organomet. Chem. 33 (2019) e4751.
- [9] R.D. Graham, D.R. Williams, J. Inorg. Nucl. Chem. 41 (1979) 1245–1249.
- [10] I.A. Zakharova, J.V. Salyn, L.V. Tatjanenko, Y.S. Mashkovsky, G. Ponticelli, J. Inorg. Biochem. 15 (1981) 89–92.
- [11] J.L. Butour, S. Wimmer, F. Wimmer, P. Castan, Chem. Biol. Interact. 104 (1997)

- 165–178.
- [12] S.V. Voitekhovich, T.V. Serebryanskaya, A.S. Lyakhov, P.N. Gaponik, O.A. Ivashkevich, *Polyhedron* 28 (2009) 3614–3620.
- [13] A. Garoufis, S.K. Hadjidakou, N. Hadjilias, *Coord. Chem. Rev.* 253 (2009) 1384–1397.
- [14] Z.D. Matović, E. Mrkalić, G. Bogdanović, V. Kojić, A. Meetsma, R. Jelić, *J. Inorg. Biochem.* 121 (2013) 134–144.
- [15] P. Castan, E. Colacio-Rodríguez, A.L. Beauchamp, S. Cros, S. Wimmer, *J. Inorg. Biochem.* 38 (1990) 225–239.
- [16] J. Ruiz, J. Lorenzo, C. Vicente, G. López, J.M. Lopez-de-Luzuriaga, M. Monge, F.X. Aviles, D. Bautista, V. Moreno, A. Laguna, *Inorg. Chem.* 47 (2008) 6990–7001.
- [17] M.A. Ali, A.H. Mirza, R.J. Butcher, M.T.H. Tarafder, T.B. Keat, A.M. Ali, *J. Inorg. Biochem.* 92 (2002) 141–148.
- [18] M.E. van der Boom, D. Milstein, *Chem. Rev.* 103 (2003) 1759–1792.
- [19] H. Li, B. Zheng, K.W. Huang, *Coord. Chem. Rev.* 293–294 (2015) 116–138.
- [20] E. Poverenov, D. Milstein, *Top. Organomet. Chem.* 40 (2013) 21–48.
- [21] H. Zhang, A. Lei, *Dalton Trans.* 40 (2011) 8745–8754.
- [22] N. Selander, K.J. Szabo, *Chem. Rev.* 111 (2011) 2048–2076.
- [23] C.J. Moulton, B.L. Shaw, *J. Chem. Soc. Dalton Trans.* (1976) 1020–1024.
- [24] C.M. Jensen, *Chem. Commun.* (1999) 2443–2449.
- [25] M. Albrecht, G. van Koten, *Angew. Chem. Int. Ed.* 40 (2001) 3750–3781.
- [26] J.L. Niu, X.Q. Hao, J.F. Gong, M.P. Song, *Dalton Trans.* 40 (2011) 5135–5150.
- [27] M. Asay, D. Morales-Morales, *Dalton Trans.* 44 (2015) 17432–17447.
- [28] H.J. Lee, S.H. Lee, H.C. Kim, Y.E. Lee, S. Park, *J. Organomet. Chem.* 717 (2012) 164–171.
- [29] C. Elamathi, R. Butcher, R. Prabhakaran, *Appl. Organomet. Chem.* 32 (2018) e4364.
- [30] P. Sathyadevi, P. Krishnamoorthy, R.R. Butorac, A.H. Cowley, N. Dharmaraj, *Inorg. Chim. Acta* 409 (2014) 185–194.
- [31] B. Bertrand, M.A. O'Connell, Z.A.E. Waller, M. Bochmann, *Chem. Eur. J.* 24 (2018) 3613–3622.
- [32] M. Muralisankar, S.M. Basheer, J. Haribabu, N.S.P. Bhuvanesh, R. Karvembu, A. Sreekanth, *Inorg. Chim. Acta* 466 (2017) 61–70.
- [33] L. Tabrizi, H. Chiniforoshan, *New J. Chem.* 41 (2017) 10972–10984.
- [34] S. Ramírez-Rave, M.T. Ramírez-Apan, H. Tlahuext, D. Morales-Morales, R.A. Toscano, J.M. Grevy, *J. Organomet. Chem.* 814 (2016) 16–24.
- [35] D.X. West, S.B. Padhye, P.B. Sonawane, *Structure and Bonding*, 76 Springer-Verlag, New York, 1991, pp. 1–49.
- [36] U. El-Ayaan, A.A.M. Abdel-Aziz, *Eur. J. Med. Chem.* 40 (2005) 1214–1221.
- [37] Z. Travnický, M. Malon, Z. Sindelar, K. Dolezal, J. Rolcik, V. Krystof, M. Strnad, J. Marek, *J. Inorg. Biochem.* 84 (2001) 23–32.
- [38] S. Radisavljević, I. Bratsos, A. Scheurer, J. Korzekwa, R. Masnikosa, A. Tot, N. Gligorijević, S. Radulović, A.R. Simović, *Dalton Trans.* 47 (2018) 13696–13712.
- [39] L. Tabrizi, H. Chiniforoshan, *RSC Adv.* 7 (2017) 34160–34169.
- [40] T. Thirunavukkarasu, H.A. Sparkes, K. Natarajan, V.G. Gnanasoundari, *Appl. Organomet. Chem.* 32 (2018) e4403.
- [41] A. Adach, M. Daszkiewicz, M. Tyszcza-Czochara, B. Barszcz, *RSC Adv.* 5 (2015) 85470–85479.
- [42] A.S. Estrada-Montano, A.D. Ryabov, A. Gries, C. Gaiddon, R.L. Lagadec, *Eur. J. Inorg. Chem.* 2017 (2017) 1673–1678.
- [43] M. Hosseini-Kharat, D. Zargarian, A.M. Alizadeh, K. Karami, M. Saeidifar, S. Khalighfard, L. Dubrulle, M. Zakariazadeh, J.P. Cloutier, Z. Sohrabijam, *Dalton Trans.* 47 (2018) 16944–16957.
- [44] Y.H. Liu, A. Li, J. Shao, C.Z. Xie, X.Q. Song, W.G. Bao, J.Y. Xu, *Dalton Trans.* 45 (2016) 8036–8049.
- [45] L. Tabrizi, L.O. Olasunkanmi, O.A. Fadare, *Dalton Trans.* 48 (2019) 728–740.
- [46] S.G. Churushova, D.V. Aleksanyan, E.Y. Rybalkina, O.Y. Susova, V.V. Brunova, R.R. Aysin, Y.V. Nelyubina, A.S. Peregodov, E.I. Gutsul, Z.S. Klemenkova, V.A. Kozlov, *Inorg. Chem.* 56 (2017) 9834–9850.
- [47] B. Boff, C. Gaiddon, M. Pfeffer, *Inorg. Chem.* 52 (2013) 2705–2715.
- [48] K. Li, T. Zou, Y. Chen, X. Guan, C.M. Che, *Chem. Eur. J.* 21 (2015) 7441–7453.
- [49] S.K. Fung, T. Zou, B. Cao, P.Y. Lee, Y.M.E. Fung, D. Hu, C.N. Lok, C.M. Che, *Angew. Chem. Int. Ed.* 56 (2017) 3892–3896.
- [50] L. Kelland, *Nat. Rev. Cancer* 7 (2007) 573–584.
- [51] T.C. Johnstone, K. Suntharalingam, S.J. Lippard, *Chem. Rev.* 116 (2016) 3436–3486.
- [52] A. Alsalmé, S. Laeeq, S. Dwivedi, M.S. Khan, K.A. Farhan, J. Musarrat, R.A. Khan, *Spectrochim. Acta A* 163 (2016) 1–7.
- [53] V.T. Yilmaz, C. Işsel, F. Suyunova, M. Aygun, B. Cevatemre, E. Ulukaya, *New J. Chem.* 41 (2017) 8092–8106.
- [54] Q. Pena, J. Lorenzo, G. Sciortino, S. Rodriguez-Calado, J.D. Marechal, P. Bayon, A.J. Simaan, O. Iranzo, M. Capdevila, O. Palacios, *J. Inorg. Biochem.* 195 (2019) 51–60.
- [55] J.M. Matés, J.A. Segura, F.J. Alonso, F. Márquez, *Arch. Toxicol.* 82 (2008) 273–299.
- [56] Y. Wang, J. Hu, Y. Cai, S. Xu, B. Weng, K. Peng, X. Wei, T. Wei, H. Zhou, X. Li, G. Liang, *J. Med. Chem.* 56 (2013) 9601–9611.
- [57] A.T. Macias, D.S. Williamson, N. Allen, J. Borgognoni, A. Clay, Z. Daniels, P. Dokurno, M.J. Drysdale, G.L. Francis, C.J. Graham, R. Howes, N. Matassova, J.B. Murray, R. Parsons, T. Shaw, A.E. Surgenor, L. Terry, Y. Wang, M. Wood, A.J. Massey, *J. Med. Chem.* 54 (2011) 4034–4041.
- [58] D. Drew, J.R. Doyle, *Inorg. Synth.* 13 (1972) 52–53.
- [59] G.B. Kauffman, D.O. Cowan, *Inorg. Synth.* 6 (1960) 211–215.
- [60] P. Skehan, R. Streng, D. Scudiero, A. Monks, J. McMahon, D. Vistica, J.T. Warren, H. Bokesch, S. Kenney, M.R. Boyd, *J. Natl. Cancer Inst.* 82 (1990) 1107–1112.
- [61] SMART and SAINT-Plus v 6.22, Bruker AXS Inc., Madison, Wisconsin, USA, 2001.
- [62] G.M. Sheldrick, *SADABS* v 2.03, University of Göttingen, Germany, 2002.
- [63] SHELXTL v 6.10, Bruker AXS, Inc, Madison, Wisconsin, USA, 2000.
- [64] P.M. Takahara, A.C. Rosenzweig, C.A. Frederick, S.J. Lippard, *Nature* 377 (1995) 649–652.
- [65] S.M.D. Rizvi, S. Shakil, M. Haneef, *EXCLI J.* 12 (2013) 831–857.
- [66] A. Pashi, F. Zunino, *Angew. Chem. Int. Ed. Eng.* 26 (1987) 615–624.
- [67] E.M. Mrkalić, R.M. Jelić, O.R. Klisurić, Z.D. Matović, *Dalton Trans.* 43 (2014) 15126–15137.
- [68] R. Schibli, K.V. Katti, W.A. Volkert, C.L. Barnes, *Inorg. Chem.* 40 (2001) 2358–2362.
- [69] S.J. Berners-Price, R.K. Johnson, A.J. Giovenella, L.F. Faucette, C.K. Mirabelli, P.J. Sadler, *J. Inorg. Biochem.* 33 (1988) 285–295.
- [70] U.K. Komarnicka, R. Starosta, A. Kyzioł, M. Jeżowska-Bojczuk, *Dalton Trans.* 44 (2015) 12688–12699.
- [71] H. Nawaz, A. Waseem, Zia-ur-Rehman, M. Nafees, M.N. Arshad, U. Rashid, *Appl. Organomet. Chem.* 31 (2017) e3771.
- [72] L.M. Broomfield, C. Alonso-Moreno, E. Martin, A. Shafir, I. Posadas, V. Ceña, J.A. Castro-Osma, *Dalton Trans.* 46 (2017) 16113–16125.
- [73] B. Dominelli, J.D.G. Correia, F.E. Kühn, *J. Organomet. Chem.* 866 (2018) 153–164.
- [74] V.T. Yilmaz, C. Işsel, O.R. Turgut, M. Aygun, M. Erkisa, M.H. Turkdemir, E. Ulukaya, *Eur. J. Med. Chem.* 155 (2018) 609–622.
- [75] P.E. Garrou, *Chem. Rev.* 81 (1981) 229–266.
- [76] X. Yang, Z.X. Wang, *Organometallics* 33 (2014) 5863–5873.
- [77] F.B. Han, Y.L. Zhang, X.L. Sun, B.G. Li, Y.H. Guo, Y. Tang, *Organometallics* 27 (2008) 1924–1928.
- [78] Y. Yoshida, S. Matsui, Y. Takagi, M. Mitani, M. Nitabaru, T. Nakano, H. Tanaka, T. Fujita, *Chem. Lett.* (2000) 1270–1271.
- [79] H. Liang, J. Liu, X. Li, Y. Li, *Polyhedron* 23 (2004) 1619–1627.
- [80] R.D. Shannon, *Acta Crystallogr. A* A32 (1976) 751–767.
- [81] S.Y. Hsu, C.H. Hu, C.Y. Tu, C.H. Lin, R.Y. Chen, A. Datta, J.H. Huang, *Eur. J. Inorg. Chem.* 2014 (2014) 1965–1973.
- [82] J. Devi, M. Yadav, D. Kumar, L.S. Naik, D.K. Jindal, *Appl. Organomet. Chem.* 33 (2019) e4693.
- [83] D.A. Megger, K. Rosowski, C. Radunsky, J. Kösters, B. Sitek, J. Müller, *Dalton Trans.* 46 (2017) 4759–4767.
- [84] L.H. Abdel-Rahman, A.M. Abu-Dief, M.R. Shehata, F.M. Atlam, A.A.H. Abdel-Mawgoud, *Appl. Organomet. Chem.* 33 (2019) e4699.
- [85] H. Steller, *Science* 267 (1995) 1445–1449.
- [86] C.B. Thompson, *Science* 267 (1995) 1456–1462.
- [87] S.J. Martin, C.P.M. Reutelingsperger, A.J. McGahon, J.A. Rader, R.C.A.A. van Schie, D.M. LaFace, D.L. Green, *J. Exp. Med.* 182 (1995) 1545–1556.
- [88] L. Zhao, Q. Wen, G. Yang, Z. Huang, T. Shen, H. Li, D. Ren, *Phytomedicine* 23 (2016) 114–122.
- [89] G. Chen, D.V. Goeddel, *Science* 296 (2002) 1634–1635.
- [90] D.W. Zhang, J. Shao, J. Lin, N. Zhang, B.J. Lu, S.C. Lin, M.Q. Dong, J. Han, *Science* 325 (2009) 332–336.
- [91] T.V. Berghe, A. Linkermann, S. Jouan-Lanhouet, H. Walczak, P. Vandenabeele, *Nat. Rev. Mol. Cell Biol.* 15 (2014) 135–147.